J. Meas. Sci. Instrum., 2025, 16(4): 486-497. http://jmsi.publish.founderss.cn
DOI: 10.62756/jmsi.1674-8042.2025047 jmsi@nuc.edu.cn

Motion intention recognition using surface electromyography and arrayed flexible thin-film pressure sensors

BU Lingyu[1], YIN Xiangguo[1,2], LIN Mingxing[1*], LIU Jiahe[3]

1. Key Laboratory of High-Efficiency and Clean Mechanical Manufacture of MOE, Nation Demonstration Center for Experimental Mechanical Engineering, School of Mechanical Engineering, Shandong University, Jinan 250061, China;
2. School of Rehabilitation Science and Engineering, University of Health and Rehabilitation Sciences, Qingdao 266071, China;
3. School of Rehabilitation Medicine, Shandong Second Medical University, Weifang 261053, China

***Corresponding author:** LIN Mingxing (mxlin@sdu.edu.cn)

Received: June 12, 2025 **Revised:** July 21, 2025 **Accepted:** September 25, 2025

Abstract: Motion intention recognition is considered the key technology for enhancing the training effectiveness of upper limb rehabilitation robots for stroke patients, but traditional recognition systems are difficult to simultaneously balance real-time performance and reliability. To achieve real-time and accurate upper limb motion intention recognition, a multi-modal fusion method based on surface electromyography (sEMG) signals and arrayed flexible thin-film pressure (AFTFP) sensors was proposed. Through experimental tests on 10 healthy subjects (5 males and 5 females, age 23±2 years), sEMG signals and human-machine interaction force (HMIF) signals were collected during elbow flexion, extension, and shoulder internal and external rotation. The AFTFP signals based on dynamic calibration compensation and the sEMG signals were processed for feature extraction and fusion, and the recognition performance of single signals and fused signals was compared using a support vector machine (SVM). The experimental results showed that the sEMG signals consistently appeared 175±25 ms earlier than the HMIF signals ($p<0.01$, paired t-test). In offline conditions, the recognition accuracy of the fused signals exceeded 99.77% across different time windows. Under a 0.1 s time window, the real-time recognition accuracy of the fused signals was 14.1% higher than that of the single sEMG signal, and the system's end-to-end delay was reduced to less than 100 ms. The AFTFP sensor is applied to motion intention recognition for the first time. And its low-cost, high-density array design provided an innovative solution for rehabilitation robots. The findings demonstrate that the AFTFP sensor adopted in this study effectively enhances intention recognition performance. The fusion of its output HMIF signals with sEMG signals combines the advantages of both modalities, enabling real-time and accurate motion intention recognition. This provides efficient command output for human-machine interaction in scenarios such as stroke rehabilitation.

Key words: upper limb rehabilitation robot; motion intention recognition; sEMG signal; arrayed flexible thin-film pressure sensor; human-machine interaction force

0 Introduction

One of the most common and severe complications following a stroke is upper limb motor dysfunction, which not only severely affects the patient's quality of life but also limits their social participation[1-5]. Rehabilitation training is an effective approach to improve motor impairments. Studies have shown that active rehabilitation training combined with motor intention recognition can improve patients' Fugl-Meyer scores by more than 30%[6]. As a rehabilitation tool that integrates mechanical structures and control algorithms, upper limb rehabilitation robots have been widely applied in clinical practice. Their training modes are mainly divided into passive and active modes[7]. In the active mode, the robot adjusts its assistive or resistive force based on the patient's motor intention, enabling active participation in the training process and thereby enhancing both effectiveness and efficiency. Therefore, accurately recognizing patients' motor intention is one of the key technologies for implementing active rehabilitation[8,9].

Motor intention recognition refers to the inference and prediction of human limb movements through the acquisition of relevant information. The real-time performance and accuracy of recognition are two critical metrics in the application of rehabilitation robots[10]. The trade-off between real-time performance

(latency $<$200 ms) and accuracy ($>$95%) is a major challenge currently faced by intention recognition technologies[11]. Sources of information for motor intention recognition typically include mechanical signals and bioelectrical signals[12]. Bioelectrical signals mainly consist of sEMG, electrooculography (EOG), and electroencephalography (EEG). Among them, sEMG signals are generated by muscle contractions and are directly related to upper limb movements. They are characterized by simple processing and high recognition accuracy, and are generated approximately 30 — 150 ms prior to actual movements, enabling good real-time performance and making them suitable for motion prediction[13].

In recent years, significant progress has been made in this field. For example, Sun et al. estimated continuous joint angles of the knee and hip based on sEMG signals using least squares support vector machines (LS-SVM) and zeroing neural networks (ZNN) [14]. Fan et al. applied transfer learning with convolutional neural networks (CNN) to knowledge learned from sEMG signals of healthy subjects, thereby improving motor intention recognition performance in individuals with distal radius amputations[15]. Zhu et al. used a multi-scale temporal convolutional network (TCN) to extract features at different temporal scales from sEMG signals and performed feature fusion, achieving better performance than traditional machine learning methods and single-scale TCN models[16]. Wang et al. used the tsfresh library to extract features from sEMG signals, selected relevant features using a random forest (RF) model, and trained a motion classification model based on the selected features[17].

However, sEMG signals also have several limitations, including low signal-to-noise ratio (SNR), susceptibility to interference, and significant individual variability. These limitations are particularly pronounced in obese individuals (BMI$>$30), where adipose tissue attenuates sEMG signals, leading to a reduction in recognition accuracy by more than 20%[18].

Mechanical signals include joint angles, angular velocities, and human-machine interaction forces (HMIF), with HMIF referring primarily to the interaction forces generated by relative motion between the human body and the exoskeleton[19]. HMIF signals offer advantages such as high signal-to-noise ratio and strong stability. Moreover, they are generated earlier than joint angle and velocity signals, enabling detection without requiring the user to complete the full motion.

Currently, several HMIF sensing devices have been implemented in practical exoskeleton systems. For example, Zhao et al. employed a novel soft skin sensor mounted on the exoskeleton linkage bracket to adjust the real-time tracking of elbow movements, thereby more accurately reflecting the user's motor intention. This new human-machine interface effectively captures the user's motion intention and enables precise control of the exoskeleton[20]. Wang et al. used pneumatic sensors to detect HMIF signals and applied an improved adaptive Kalman filter to reduce signal noise, time delays, and eliminate occasional errors through clipping filtering. Experimental results demonstrated that the designed intention recognition system could accurately identify human-machine interaction information[21]. Feng et al. proposed a motor intention acquisition method based on static torque sensors, which can effectively capture patients' voluntary motion intentions. With this method, rehabilitation robots can provide more natural and personalized assistance according to patient intentions[22]. Li et al. aiming to encourage patients' active participation in rehabilitation, utilized a three-dimensional force sensor to collect interaction forces during training and input these data into a fuzzy inference system for motion intention recognition[23]. However, HMIF signals are generated after the human-machine interaction begins, resulting in insufficient real-time performance. Therefore, combining sEMG signals with HMIF signals has emerged as a more promising solution[24].

Some researchers have combined mechanical signals with bioelectrical signals to develop a multi-source signal-based human-machine interaction interface, achieving promising results. Choi et al. used sEMG, force-sensitive resistors (FSR), and inertial measurement units (IMU) to collect upper limb signals. These weAR-MobileNetV2 architectures achieved a recognition accuracy of 95% and an $F1$ score of 0.95[25]. Pan et al. combined the contact state between the hand and the robotic joint with sEMG signals to recognize motion intention for controlling the robot's movement[26]. López Molina combined upper limb accelerometer (ACC) data with EMG signals, achieving a prediction accuracy ranging from 75.80% to 91.01% for distinguishing between "stationary" and "movement" states[27]. Fang et al. fused sEMG signals and acceleration (ACC) signals using a multimodal deep forest (MMDF) framework to recognize hand movements, demonstrating that ACC signals serve as an excellent complement to sEMG[28]. However, none of them integrated sEMG with pressure.

This study proposed an upper limb motion intention recognition method based on sEMG and an AFTFP sensor. The AFTFP sensor features low cost (which costs only

about 1/10 as much as conventional force/torque sensors), easy integration, and high-density array design, enabling it to capture richer human-machine interaction force (HMIF) information compared to traditional force/torque sensors. The sEMG signals reflect the electrical activity of muscles prior to movement initiation, providing early information about the user's motion intention, while the AFTFP sensors capture the distribution of contact pressure between the limb and the device during motion execution, reflecting the actual physical interaction process. The fusion of the two enables dual perception of intention and feedback, thereby enhancing the robustness and accuracy of motion intention recognition.

In this study, the sensor was embedded into the fixation sleeve of a rehabilitation robot to collect HMIF signals from the patient's arm and sEMG signals from the forearm. By performing signal preprocessing, feature extraction, and feature fusion on both signals, a support vector machine (SVM) was employed to classify different motion actions.

The main contributions of this study were as follows. 1) The AFTFP sensor was applied for the first time to upper limb motion intention recognition, providing a low-cost and high-accuracy HMIF measurement solution. 2) A multimodal fusion recognition method based on sEMG and HMIF signals was proposed, combining the anticipatory nature of sEMG with the stability of HMIF signals. 3) The system achieved an end-to-end delay of less than 100 ms, meeting real-time requirements.

This research provided an efficient and reliable motion intention recognition method for active rehabilitation training in stroke patients, with significant clinical implications and application value.

1 Materials and methods

1.1 Experimental overview

This study aimed to propose a multimodal motion intention recognition method based on sEMG and AFTFP sensors, addressing the trade-off between real-time performance and reliability in traditional intention recognition systems. The experimental design was grounded in the theory of multimodal signal fusion, combining the anticipatory nature of sEMG signals with the stability of human-machine interaction force (HMIF) signals to achieve real-time and accurate intention recognition in upper limb rehabilitation robots.

The experiment began with the acquisition of sEMG and HMIF signals from subjects performing various motion intentions. The offline collected signals were then subjected to several processing steps, including preprocessing, signal segmentation, feature extraction, feature fusion, and classification[29]. Finally, by comparing the recognition performance of single-modality signals and fused signals, the effectiveness of the proposed method was validated.

1.2 Signal acquisition system

1.2.1 sEMG sensor

The sensor used in this experiment to collect upper limb sEMG signals was a single-channel sEMG sensor with dimensions of 2.54 cm×2.54 cm, as shown in Fig.1.

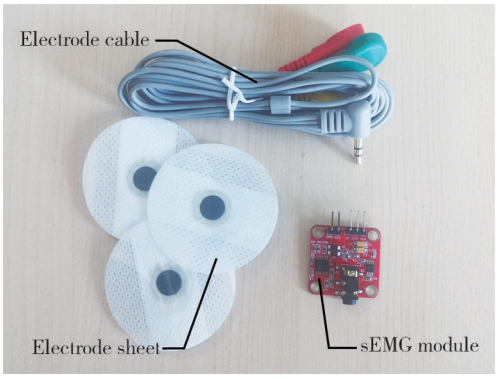

Fig. 1 Single-lead electromyography sensor

This sensor is built using the AD8221 chip from Analog Devices Inc. (ADI), which features high input impedance (>10^{12} Ω) and a high common-mode rejection ratio (CMRR>100 dB). It provides adjustable amplification of sEMG signals, with a gain range from 100 times to 1 000 times. Additionally, it performs rectification of muscle electrical signals through filtering and output a voltage signal ranging from 0 to Vs volts, with the amplitude depending on the activity level of the targeted muscle. The output data from this module is a calibrated signal that had been amplified and smoothed via an analog-to-digital converter (ADC).

The frequency components of sEMG signals typically range from 20 Hz to 500 Hz[30], depending on factors such as electrode spacing, subcutaneous fat content, and muscle type. Therefore, the sampling frequency of the sEMG sensor was set to 1 kHz to satisfy the Nyquist sampling theorem. Ag/AgCl electrodes were used and placed according to the SENIAM standard on the long head of the biceps brachii and the lateral head of the triceps brachii, with electrode-skin impedance maintained below 10 kΩ.

1.2.2 AFTFP sensor

The AFTFP sensor used in the experiment is shown in Fig. 2. This sensor is fabricated by transferring nanostructured piezoresistive materials, silver paste, and

other components onto a flexible film substrate (thickness: 0.2 mm) using precision printing technology, followed by drying and curing. It features a sensitivity of 1.2 mV/N, a linearity of $R^2>0.98$, and a hysteresis error of less than 4.2%.

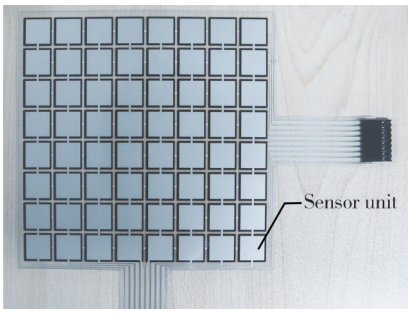

Fig. 2 Single AFTFP sensor

When pressure is applied to the sensor, its resistance decreases with increasing pressure. The sensor exhibits a piezoresistive characteristic where resistance follows a power-law relationship with pressure, and the reciprocal of resistance shows an approximately linear relationship with pressure. Hardware and software are used to process and convert the data to obtain the corresponding force values.

The RX-M64 is a general-purpose AFTFP sensor with a 8×8 array design, comprising 64 independent sensing units. Each unit is a square with a side length of 12 mm. The sensor has a measurement range of 1.0—50 kg and overall dimensions of 125 mm×125 mm.

To capture pressure information from multiple directions, two thin-film pressure sensors are bent and attached to the inner surface of the sleeve[31], as shown in Fig. 3. The sleeve was fabricated using 3D printing technology with PETG material. In this setup, the axial direction of the sleeve was designated as the columns of the AFTFP sensor, while the radial direction was designated as the rows.

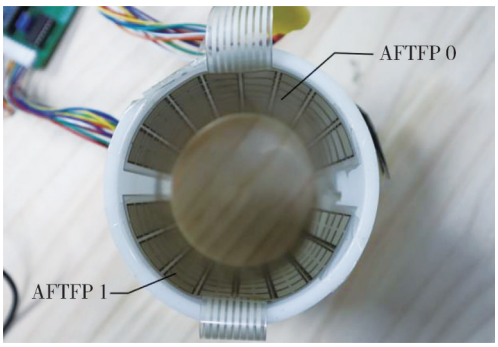

Fig. 3 Sleeve with two-piece arrayed AFTFP sensor

As shown in Fig. 4, the pressure distribution signals collected by the AFTFP sensors essentially reflect the mechanical interactions between the skin and the sensor array caused by muscle contractions or limb movements. During upper limb movements, the contraction of the agonist muscles led to changes in contact between the upper limb and the AFTFP, resulting in variations in surface pressure distribution. The magnitude and spatial characteristics of these pressure changes were closely related to the force generated by the muscles, as well as the amplitude and speed of joint movements.

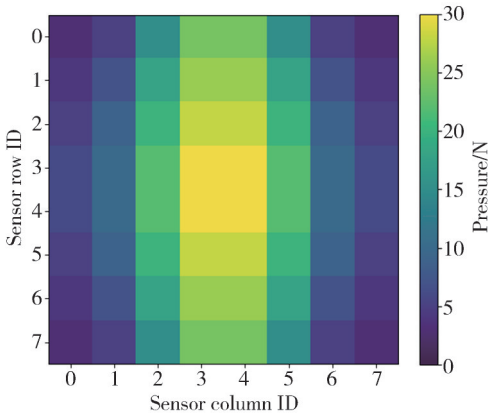

Fig. 4 Pressure distribution map of AFTFP sensor

1.3 Signal acquisition

This study strictly adhered to the ethical principles outlined in the Declaration of Helsinki. Prior to the start of the experiment, all participants signed informed consent forms after being fully informed of the study's purpose, procedures, and potential risks.

Four upper limb movements with relatively high recognition accuracy were selected as target actions: elbow flexion/extension and shoulder external/internal rotation. For each movement, five sets of data were collected, with each set containing 10 repetitions. Each movement lasted 1.5 s, followed by a 1.5-second interval. A one-minute rest was provided between sets to prevent fatigue and discomfort[32].

Ten healthy subjects (5 male and 5 female; age 23±2 years) were recruited. Two sEMG sensors were attached to the biceps brachii and triceps brachii of the upper limb. The subject's forearm is inserted into a sleeve fixed on the robotic arm, as shown in Fig.5.

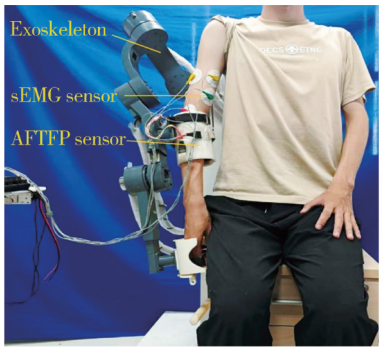

Fig. 5 Position of sensors relative to upper limb

During data collection, participants were not required to complete the full range of motion but were instructed to perform the corresponding movement trend as prompted on the computer screen.

1.4 Signal preprocessing

1.4.1 sEMG signal preprocessing

The useful information in sEMG signals is primarily distributed within the 20—500 Hz frequency range, with the main energy concentrated between 20 Hz and 150 Hz[33]. However, sEMG signals acquired during data collection are inevitably contaminated by various types of noise, such as high-frequency noise, power line interference, and baseline drift[34], which complicated the extraction of meaningful features. Therefore, effective denoising are required before further processing of sEMG signals.

To address this, a band-pass filter with a frequency range of 20 — 150 Hz and a notch filter at 50 Hz were designed to remove high-frequency noise and power line interference, respectively, thereby obtaining the raw sEMG signal. The band-pass filter is

$$H(s)=\frac{\omega_2 s}{s^2+(\omega_2-\omega_1)s+\omega_1\omega_2}, \tag{1}$$

where $\omega_1=2\pi f_1$ is the angular frequency of the lower cutoff (20 Hz), $\omega_2=2\pi f_2$ is the angular frequency of the upper cutoff (150 Hz), and s is the complex frequency variable.

1.4.2 HMIF signal preprocessing

Each flexible thin-film pressure sensor contained 64 channels of data. To reduce redundant data, this experiment selected the 1st, 3rd, 5th, and 7th columns of each sensor as the effective human-machine interaction force (HMIF) data.

Due to the bending of the AFTFP sensor, internal stress was generated, causing significant fluctuations in the HMIF signals. To process the HMIF signals more accurately, a dynamic calibration compensation method was employed.

First, the mean value of each column's data is taken as the sample value, calculated by

$$F_i=\frac{1}{8}\sum_{j=1}^{8}F_{ij},\ i=1,3,5,7, \tag{2}$$

where F_i is the sample value, F_{ij} is the original value of each unit, i is the column index, and j is the row index.

Then, a "baseline subtraction" method was employed: baseline pressure data under no external force (containing only internal stress) was first collected, and then this baseline was subtracted from real-time raw pressure data to isolate and remove internal stress interference, leaving only the external load signal. The correction formula used is

$$\tilde{F}_k=F_k-F_0, \tag{3}$$

where F_k denotes the original sample value at time k, F_0 represents the initial stress-free value, and $\tilde{F}_k$ is the corrected sample value. Through correction, the accuracy of the AFTFP signals were significantly improved, providing a reliable data foundation for subsequent feature extraction and fusion.

After the above preprocessing, each AFTFP sensor yielded 4 channels of HMIF signals, and two sensors provided a total of 8 channels of HMIF signals.

1.5 Signal segmentation

1.5.1 sEMG signal segmentation

Since the acquisition process was continuous, each signal segment contained both active and rest periods. Therefore, before feature extraction, it was necessary to segment the active periods. According to the literature, sEMG signals exhibited a certain degree of anticipation. To fully utilize this characteristic, the start points of both HMIF and sEMG signals were searched separately.

For sEMG signals, the energy threshold method was used to locate the start point[35]. The average energy at each point was calculated using a sliding window, and an appropriate threshold was selected empirically. The sliding window energy calculation formula can be expressed as

$$E_t=\frac{1}{W}\sum_{i=t-W+1}^{t}\left(x_i^2+y_i^2\right). \tag{4}$$

When $E_t>\alpha\cdot E_{\text{baseline}}$, the segment is classified as an active segment (where α is the threshold coefficient and E_{baseline} is the baseline energy mean, both selected based on experience). W represents the window size ($W=100$).

1.5.2 HMIF signal segmentation

Considering that the slope of the HMIF signal changed abruptly in active segments, forward differences were used to calculate the slope at each point of the HMIF signal. A threshold was then set to detect the onset point of the signal. The forward difference of slope is caculated by

$$\Delta F_t=F_{t+1}-F_t. \tag{5}$$

The segment was classified as active when $|\Delta F_t|>\beta\cdot\sigma\Delta F$, where β is the sensitivity coefficient and $\sigma\Delta F$ is the standard deviation of the slope during the resting segment.

1.5.3 Signal segmentation results

The onset point of the sEMG signal was used as the starting point of the fusion scheme. The segmented signals are shown in Fig. 6. HMIF 0 corresponded to

AFTFP 0, and HMIF 1 corresponded to AFTFP 1. sEMG1 represented the sEMG signal of the triceps brachii, while sEMG2 represented the sEMG signal of the biceps brachii. The red dashed line indicated the start time of the movement, and the green dashed line indicated the end time of the movement.

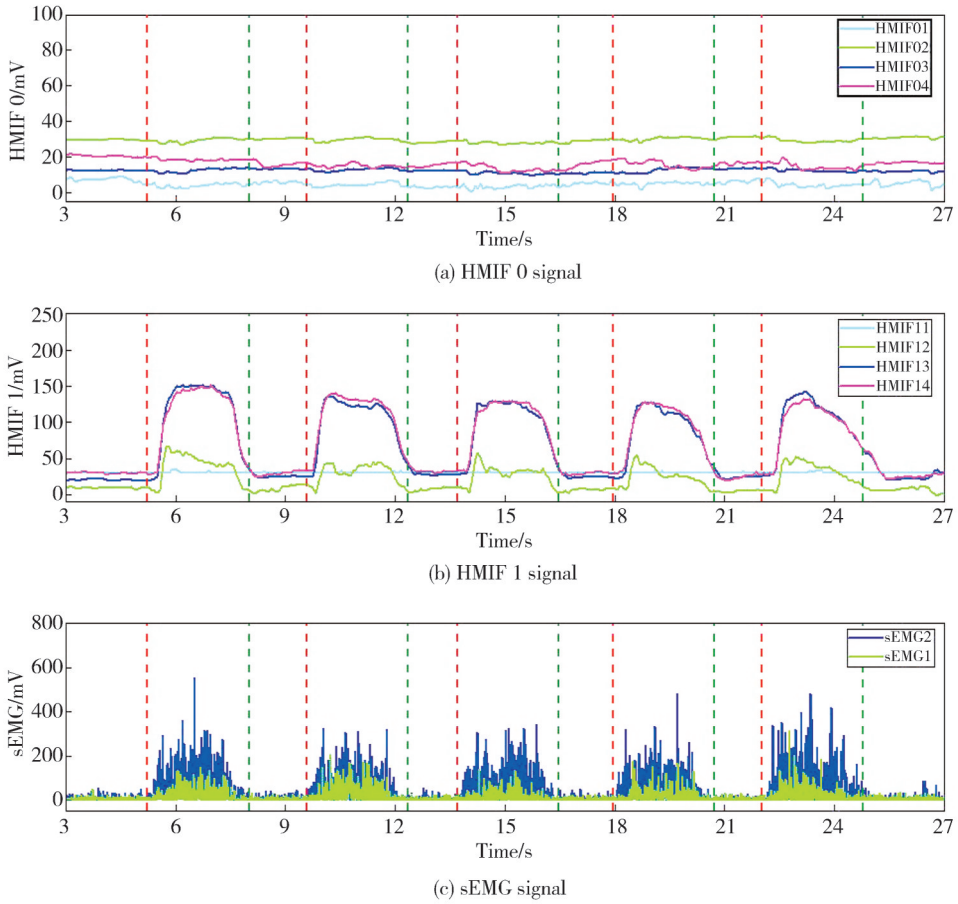

(a) HMIF 0 signal

(b) HMIF 1 signal

(c) sEMG signal

Fig. 6 Results of segmenting HMIF and sEMG signals generated during upper limb flexion using the energy threshold method

1.6 Feature extraction

The preprocessed signals can't be directly used for classifier recognition. Therefore, feature extraction is necessary. The extracted features are then fed into the classifier for training and classification.

In the process of feature extraction, a sliding time window and an incremental window are typically used for extracting features from sEMG signals. To evaluate the real-time performance of the fusion scheme, different window sizes were employed in this study: 0.1 s, 0.3 s, 0.5 s, and 0.8 s, with a 50% overlap rate.

1.6.1 sEMG signal feature extraction

For sEMG signals, features can be extracted from the time domain, frequency domain, and time-frequency domain. To reduce computational complexity, several typical time-domain features were selected in this study, including mean absolute value (MAV), slope sign changes (SSC), waveform length (WL), variance (VAR), root mean square (RMS), wilson amplitude, kurtosis, and skewness, a total of nine features[36]. The computation methods of some features are listed in Table 1. A total of 18 features were extracted from the signals of the two sEMG sensors within each time window.

Table 1 Partial time-domain features of sEMG

Time-domain feature	Calculation formula
Mean absolute value (MAV)	$F_1=\frac{1}{N}\sum_{i=1}^{N}\lvert x_i\rvert$
Slope sign changes (SSC)	$F_2=\sum_{i=2}^{N-1}f(x_i)$
Waveform length (WL)	$F_3=\sum_{i=1}^{N-1}\lvert x_{i+1}-x_i\rvert$

1.6.2 HMIF signal feature extraction

For the HMIF signals, the MAV was selected as the feature for each signal. Accordingly, within a single time window, a total of eight features were extracted from all HMIF signals. The MAV of HMIF is calculated by

$$F_{\mathrm{HMIF}}=\frac{1}{N}\sum_{i=1}^{N}\lvert x_i\rvert. \tag{6}$$

The feature extraction process was accelerated through parallel computing to ensure real-time performance.

1.7 Data fusion

Multi-sensor data fusion is categorized into three levels: data-level fusion, feature-level fusion, and decision-level fusion.

Data-level fusion directly combines the raw data collected from different sensors and represents the lowest level of fusion. Its advantage lies in providing more detailed information. However, due to the large volume of data, it incurs high processing costs and suffers from poor real-time performance.

Feature-level fusion involves extracting representative features from each sensor's data and combining them into a single feature vector. This approach requires less communication bandwidth but can suffer from reduced accuracy due to information loss during feature extraction.

Decision-level fusion processes data from each sensor independently to derive preliminary decisions, which are then combined using certain rules and confidence measures to produce an optimal final decision. While this method requires the least communication bandwidth, its accuracy is typically lower compared to the other two approaches.

Considering the real-time performance and reliability required for motion intention recognition, this study adopted feature-level fusion. Specifically, the features extracted from sEMG and HMIF signals were concatenated into a 24-dimensional feature vector. Feature-level fusion ensured real-time capability while fully leveraging the complementary characteristics of multimodal signals.

1.8 Classifier

In this study, the support vector machine (SVM) was chosen as the feature classifier. SVM is a supervised learning model based on statistical learning theory, and its core idea is to classify data by constructing an optimal hyperplane. For binary classification problems, SVM searches for a separating hyperplane by maximizing the margin between classes. For multi-class classification problems (with four action categories in this study), the "one-vs-one" strategy is employed, in which multiple binary classifiers are constructed and a voting mechanism is used to make the final decision. Compared to other classifiers, SVM demonstrates stronger generalization ability, especially in scenarios with small sample sizes and high-dimensional data.

For linearly separable data, SVM finds the optimal hyperplane by solving the convex optimization problem, that is

$$\min_{\boldsymbol{w},b} \frac{1}{2}\|\boldsymbol{w}\|^2, \text{ s.t. } y_i(\boldsymbol{w}^{\mathrm{T}}\boldsymbol{x}_i + b) \geqslant 1, \ \forall i. \tag{7}$$

For nonlinear data, slack variables $\boldsymbol{\xi}_i$ and a regularization parameter C are introduced to formulate the soft-margin optimization problem, that is

$$\min_{\mathrm{w},b,\xi} \frac{1}{2}\|\boldsymbol{w}\|^2 + C\sum_{i=1}^{n}\boldsymbol{\xi}_i,$$
$$\text{s.t. } y_i(\boldsymbol{w}^{\mathrm{T}}\boldsymbol{x}_i + b) \geqslant 1 - \boldsymbol{\xi}_i, \quad \boldsymbol{\xi}_i \geqslant 0, \quad \forall i. \tag{8}$$

By using the kernel trick, data is mapped into a high-dimensional space, and the decision function is

$$f(\boldsymbol{x}) = \mathrm{sgn}\left(\sum_{i=1}^{N} \alpha_i y_i K(\boldsymbol{x}_i, \boldsymbol{x}_j) + b\right), \tag{9}$$

where α_i denoted the Lagrange multipliers. In this study, the radial basis function (RBF) kernel is used, that is

$$K(\boldsymbol{x}_i, \boldsymbol{x}_j) = \exp(-\gamma\|\boldsymbol{x}_i - \boldsymbol{x}_j\|^2). \tag{10}$$

The hyperparameters were optimized using grid search, with the optimal combination determined as $C=10$ and $\gamma=0.01$.

The extracted sEMG signal features (18-dimensional), HMIF signal features (8-dimensional), and fused features (24-dimensional) were separately input into the SVM classifier.

Model performance was evaluated using five-fold cross-validation. The classification accuracy calculated from the confusion matrix can be defined by

$$\frac{\Sigma_{k=1}^{4} P_k}{N_{\text{total}}} \times 100\%, \tag{11}$$

where P_k represents the number of correctly classified samples for the k class, and N_{total} is the total number of samples.

2 Results

2.1 Analysis results of sEMG and HMIF signals

To demonstrate the time difference in the occurrence of HMIF and sEMG signals, the onset points of the active segments in both signals were separately detected and segmented. The segmentation results are shown in Fig.7.

The dashed lines in Fig.7 represent the start time of different signals. The blue dashed line indicate the onset of the sEMG signal, while the red dashed line indicate the onset of the HMIF signal. It can be observed that the sEMG signal began before the HMIF signal appears, which is consistent with the leading characteristic of the sEMG signal. Experiments are conducted on all four types of movements, and the resulting lead time is shown in Fig.8.

As shown in Fig.8, the average advance time is between 140 ms and 250 ms. This indicates that, compared to using the HMIF signals alone, the incorporation of sEMG signals

advanced the recognition time by 140 ms to 250 ms. This lead time facilitated earlier prediction of the patient's movements, compensating for the delay inherent in the HMIF signals.

Analysis of all experimental samples across the four motions shows that the sEMG signals consistently appear 175±25 ms earlier than the HMIF signals. To verify the significance of this advance time, a paired *t*-test was conducted, yielding $p<0.01$, which indicated a statistically significant difference in advance time between the sEMG and HMIF signals. This result further confirmed the leading characteristic of sEMG signals in movement intention recognition, providing a theoretical basis for multimodal fusion.

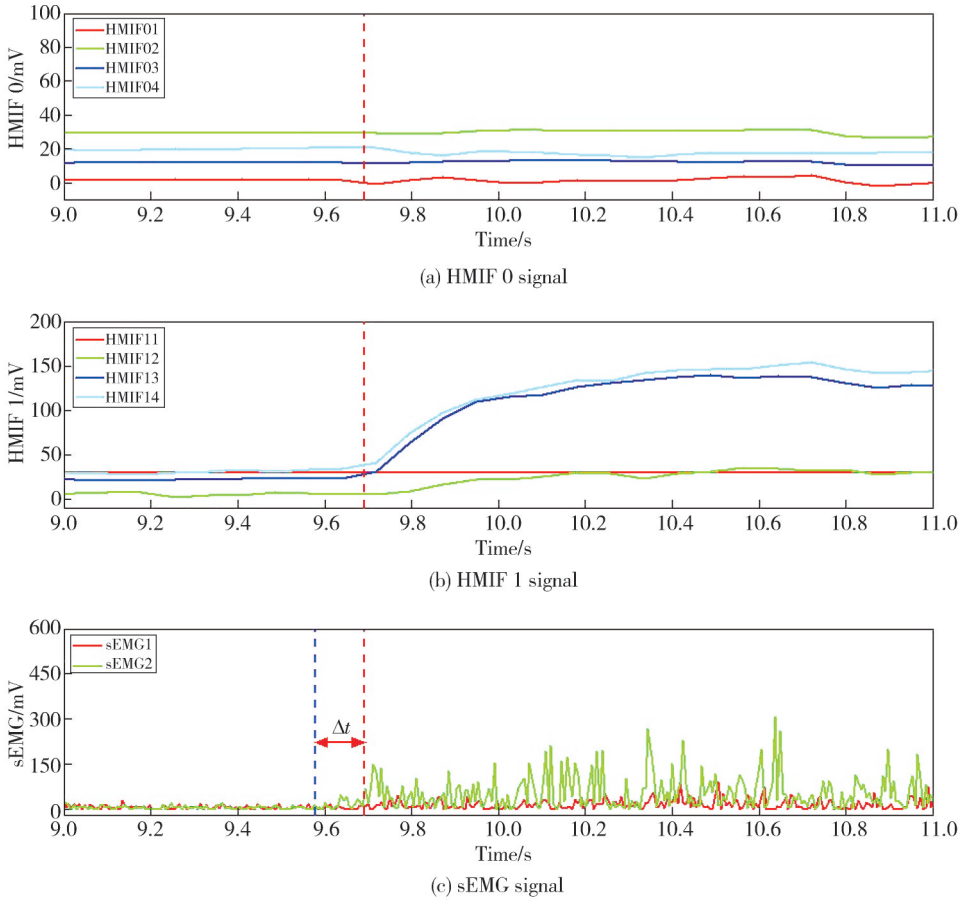

Fig. 7 Start time of HMIF signals and sEMG signals

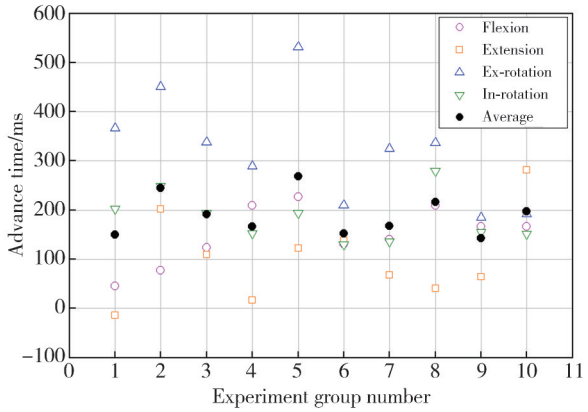

Fig. 8 Advance time of sEMG signals relative to HMIF signals in different experimental groups

2.2 Recognition results under offline conditions with different window sizes

The offline condition refers to training and testing based on features extracted from the entire signal segment. Specifically, features were sequentially extracted from each window of the signal using fixed-size windows and sliding windows for both training and testing. The corresponding real-time condition used features extracted from the entire signal segment for training, consistent with the offline training, while only the features from the first window were used during testing.

Using the onset of the sEMG signal as the start of the active segment, features were extracted separately from the sEMG and HMIF signals. Subsequently, the sEMG features, HMIF features, and fused features were input into an SVM classifier. The recognition results are shown in Fig.9.In Fig.9, the classification accuracies of the sEMG signals are 88.09%, 94.44%, 96.15%, and 97.7%, respectively. The accuracy are gradually improved with the increase of the time window length. However, continuously

increasing the window size to pursue higher accuracy results in greater time delay. The recognition accuracy of the HMIF signals is relatively high and remains stably around 99.0%. For a 0.1-second window, the average recognition accuracy using only sEMG signals is 88.09%, while after introducing the HMIF signals, the recognition accuracy of the fused signals increases to 99.77%. Similar results are observed for other window sizes, with accuracy stabilizing around 99.8% as the window length increases. Therefore, the 0.1-second window balances high accuracy and reduces delay. These results indicated that the combination of HMIF and sEMG signals improved recognition accuracy and enhanced the system's real-time performance and accuracy even within shorter time windows.

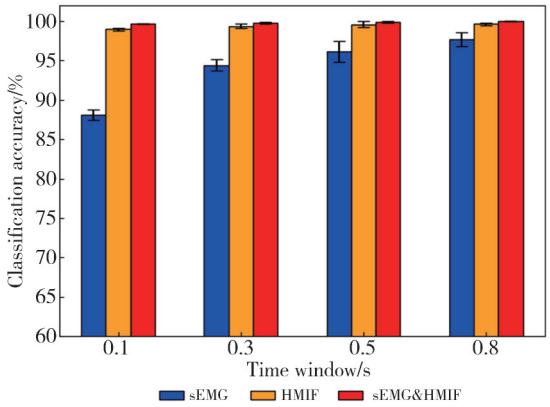

Fig. 9 Classification accuracy of three recognition schemes for time window of different lengths

2.3 Recognition results under real-time conditions with different window sizes

For real-time recognition, the accuracy of the first time window was particularly critical. Based on the onset of the sEMG signal's active segment, the time window lengths are also chosen as 0.1 s, 0.2 s, 0.3 s, and 0.5 s. The recognition results of the three schemes in the first time window are shown in Fig.10.

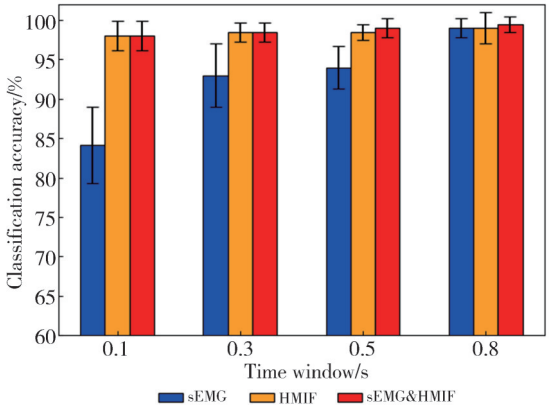

Fig. 10 Classification accuracy of the first time window for three recognition schemes for time window of different lengths

Fig.10 shows that the trend of recognition results in the first time window is similar to that in Fig.9, maintaining the same pattern. Additionally, under different time window lengths, the recognition accuracy of the sEMG signals in the first time window is consistently lower than the average recognition accuracy shown in Fig.10. Specifically, when the time window was 0.1 s, the recognition accuracy of the sEMG signals in the first time window is only 84.1%. Such a relatively low accuracy might have led to serious accidents. However, by introducing the HMIF signals, the recognition accuracy is improved to 98.2%, representing a 14.1% increase. This significantly reduced the likelihood of accidents, greatly enhanced the safety of the real-time system, and the 0.1 s time window enabled the end-to-end delay in real-time recognition to be controlled within 100 ms.

2.4 Recognition results of different actions with the same time window under real-time conditions

The models' recognition accuracy varies across different actions. Analyzing the recognition accuracy for each action helps target improvements in model performance. The confusion matrix was calculated using the first time window with a time window length of 0.1 s. The results are shown in Fig.11.

Fig.11(a) shows the recognition results using only the sEMG signals, while Fig.11(b) displays the results for the fused signals. The confusion matrices indicate that, whether using single sEMG signals or multi-signal fusion, the recognition accuracy for the flexion action is the lowest. However, the fused signals achieve 100.0% accuracy for the extension and external rotation actions, and 96.0% accuracy for the flexion and internal rotation actions. This demonstrated that the model performed well.

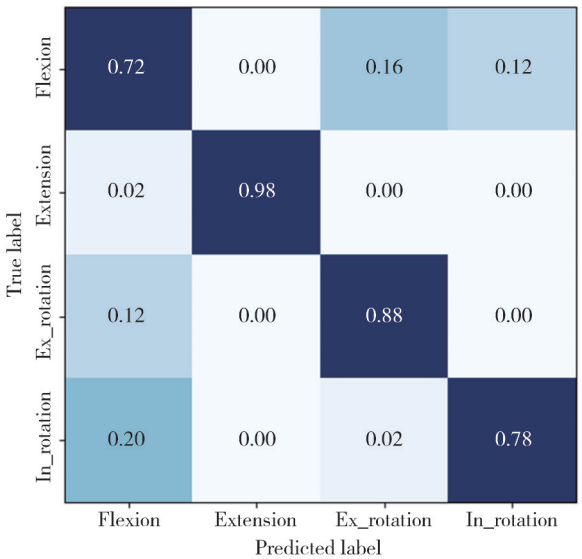

(a) Based on single sEMG signal

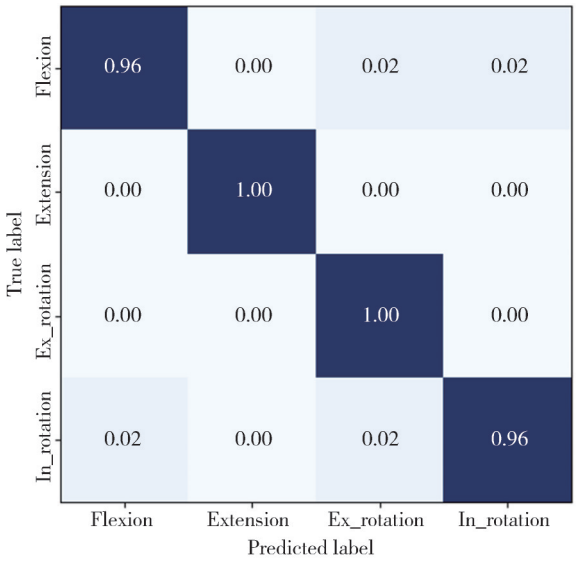

(b) Based on fused signal (sEMG and HMIF)

Fig. 11 Confusion matrix of classification results for the first time window of four actions based on different recognition schemes

3 Discussion

The real-time performance and accuracy of motion intention recognition have always been key issues limiting its further practical application. Combining sEMG signals with HMIF signals is an effective solution. Additionally, sensor cost is also an important factor.

HMIF signals can provide extremely high recognition accuracy, which in this experiment remains stable around 99.0%. However, using HMIF signals alone leads to recognition delays, which is unfavorable for real-time human-machine interaction in active training. Moreover, traditional force sensors are costly and complex to install, sometimes requiring redesign of the robotic arm structure to capture interaction force signals, which limits the number of recognizable actions due to dimensional constraints. sEMG signals inherently precede the motion by 30—150 ms, enabling prediction of actions. However, due to high noise and susceptibility to interference, sEMG signals have relatively lower recognition accuracy. Furthermore, using sEMG signals alone requires complex filtering and feature extraction to ensure high accuracy, which undoubtedly reduces real-time performance.

During actual data collection, multiple electrodes need to be placed to capture sufficient signals for recognition, which can cause discomfort for the subjects. By combining sEMG and HMIF signals, the system can determine the onset of the motion signal through the energy of the sEMG signal, preserving the real-time characteristic of sEMG and enabling early motion prediction. The inclusion of HMIF signals improves the accuracy of sEMG signals across all time windows, reaching nearly 100%, while allowing the recognition window size to be shortened. This enhances system safety and further strengthens real-time performance. On the other hand, introducing the AFTFP sensor and reducing the number of sEMG electrodes makes the data acquisition process more natural and reduces subject discomfort. The 64-channel AFTFP sensor can recognize multiple motions, and future training models can identify more complex actions to adapt to practical application scenarios.

In the classification process, flexion motions may be misclassified as internal or external rotation, and internal rotation may be misclassified as flexion. This could be related to the placement of sEMG sensors and the subjects' force application patterns, suggesting that sensor placement should be further optimized. Nevertheless, the fused signals achieve classification accuracy above 95% for all four actions, even reaching 100%, indicating that the SVM classification model based on fused signals performs well and has practical application potential.

In summary, the fusion scheme retains the advantages of both types of signals while avoiding their drawbacks, helping to promote further applications of intention recognition.

4 Conclusions

This study proposed a multimodal fusion method based on sEMG and AFTFP sensors for motion intention recognition in upper limb rehabilitation robots. Experimental results demonstrated that the fusion of sEMG and HMIF signals effectively combined the advantages of both, significantly improving recognition performance.

The innovations of this study include: 1) the first application of the AFTFP sensor in motion intention recognition, providing a low-cost, high-density HMIF measurement solution; 2) the proposal of a multimodal fusion method based on sEMG and HMIF signals, combining the anticipatory nature of sEMG with the stability of HMIF; 3) the realization of high-accuracy and low-latency intention recognition through dynamic calibration compensation and feature-level fusion techniques. The introduction of the AFTFP sensor not only reduces system cost but also decreases the number of sEMG sensors required, thereby enhancing subject comfort.

In the future, further optimization of sensor placement and classification algorithms can extend this method to recognize more complex motions. Additionally, combining brain-computer interface (BCI) technology holds promise for deep fusion of multimodal signals (e.g., sEMG+HMIF+EEG), providing more flexible and intelligent human-machine interaction solutions for rehabilitation robots.

In summary, this study provided an efficient and reliable method for motion intention recognition in upper limb rehabilitation robots, with significant clinical relevance and application prospects, offering new ideas to advance rehabilitation robot technology.

Acknowledgement

This work was supported by Guangdong Basic and Applied Basic Research Foundation (No. 2024A1515012810).

Declaration of conflicting interests

The authors have no conflict of interests related to this publication.

References

[1] Report on Stroke Center in China Writing Group. Brief report on stroke center in China, 2022. Chinese Journal of Cerebrovascular Diseases, 2024, 21(8): 565-576.

[2] SHEN S Y, CHU T C, WANG J, et al. Progress in the application of motor imagery therapy in upper limb motor function rehabilitation of stroke patients with hemiplegia. Frontiers in Neurology, 2025, 16: 1454499.

[3] ANWER S, WARIS A, GILANI S O, et al. Rehabilitation of upper limb motor impairment in stroke: a narrative review on the prevalence, risk factors, and economic statistics of stroke and state of the art therapies. Healthcare, 2022, 10(2): 190.

[4] TANG Q Q, YANG X Y, SUN M M, et al. Research trends and hotspots of post-stroke upper limb dysfunction: a bibliometric and visualization analysis. Frontiers in Neurology, 2024, 15: 1449729.

[5] WANG D, WANG J, ZHAO H B, et al. The relationship between the prefrontal cortex and limb motor function in stroke: a study based on resting-state functional near-infrared spectroscopy. Brain Research, 2023, 1805: 148269.

[6] SULLIVAN J L, BHAGAT N A, YOZBATIRAN N, et al. Improving robotic stroke rehabilitation by incorporating neural intent detection: Preliminary results from a clinical trial//2017 International Conference on Rehabilitation Robotics, July 17-20, 2017, London, UK. New York: IEEE, 2017: 122-127.

[7] YANG Y M. Research on active-passive training control strategies for upper limb rehabilitation robot. Machines, 2024, 12(11): 784.

[8] CHENG L, XIA X Z. A survey of intelligent control of upper limb rehabilitation exoskeleton. Robot, 2022, 44(6): 750-768.

[9] LUO S L, MENG Q L, LI S J, et al. Research of intent recognition in rehabilitation robots: a systematic review. Disability and Rehabilitation: Assistive Technology, 2024, 19(4): 1307-1318.

[10] MIAO M D, GAO X S, ZHAO J, et al. Rehabilitation robot following motion control algorithm based on human behavior intention. Applied Intelligence, 2023, 53(6): 6324-6343.

[11] AI Q S, LIU Z M, MENG W, et al. Machine learning in robot-assisted upper limb rehabilitation: a focused review. IEEE Transactions on Cognitive and Developmental Systems, 2023, 15(4): 2053-2063.

[12] SONG Z Q, ZHAO P, WU X J, et al. An active control method for a lower limb rehabilitation robot with human motion intention recognition. Sensors, 2025, 25(3): 713.

[13] SONG T, ZHANG K P, YAN Z, et al. Research on upper limb motion intention classification and rehabilitation robot control based on sEMG. Sensors, 2025, 25(4): 1057.

[14] SUN Z B, ZHANG X, LIU K P, et al. A multi-joint continuous motion estimation method of lower limb using least squares support vector machine and zeroing neural network based on sEMG signals. Neural Processing Letters, 2023, 55(3): 2867-2884.

[15] FAN J H, JIANG M Z, LIN C, et al. Improving sEMG-based motion intention recognition for upper-limb amputees using transfer learning. Neural Computing and Applications, 2023, 35(22): 16101-16111.

[16] ZHU Y X, LI X, WANG J H, et al. A multi-scale temporal convolutional network-based method for sEMG upper limb motion intention recognition//2022 5th International Conference on Intelligent Robotics and Control Engineering, September 23-25, 2022, Tianjin, China. New York: IEEE, 2022: 113-117.

[17] WANG F Y, ZHANG D H, LI Z Y, et al. Method for sEMG-based motion recognition for patients at different brunnstrom stages. Robot, 2020, 42(6): 661-671.

[18] LOBOV S, KRILOVA N, KASTALSKIY I, et al. Latent factors limiting the performance of sEMG-interfaces. Sensors, 2018, 18(4): 1122.

[19] YANG X, WANG J C, GAO C, et al. Research on human machine interaction of exoskeleton. Advances in Engineering Technology Research, 2023, 8(1): 859.

[20] ZHAO Z R, LI X, LIU M F, et al. A novel human-robot interface based on soft skin sensor designed for the upper-limb exoskeleton. Proceedings of the Institution of Mechanical Engineers, Part C: Journal of Mechanical Engineering Science, 2022, 236(1): 566-578.

[21] WANG W D, LI H H, XIAO M H, et al. Design and verification of a human-robot interaction system for upper limb exoskeleton rehabilitation. Medical Engineering & Physics, 2020, 79: 19-25.

[22] FENG Y F, WANG H B, VLADAREANU L, et al. New motion intention acquisition method of lower limb

rehabilitation robot based on static torque sensors. Sensors, 2019, 19(15): 3439.
[23] LI G N, TAO L, MENG J Y, et al. Research on mode adjustment control strategy of upper limb rehabilitation robot based on fuzzy recognition of interaction force. Journal of Biomedical Engineering, 2024, 41(1): 90-97.
[24] LI K X, ZHANG J H, WANG L F, et al. A review of the key technologies for sEMG-based human-robot interaction systems. Biomedical Signal Processing and Control, 2020, 62: 102074.
[25] CHOI A, HYONG K, CHAE S, et al. Improved transfer learning for detecting upper-limb movement intention using mechanical sensors in an exoskeletal rehabilitation system. IEEE Transactions on Neural Systems and Rehabilitation Engineering, 2024, 32: 3953-3965.
[26] PAN Y, CHEN C J, ZHAO Z X, et al. Robot teaching system based on hand-robot contact state detection and motion intention recognition. Robotics and Computer-Integrated Manufacturing, 2023, 81: 102492.
[27] LÓPEZ MOLINA J A. Motion intention estimation using sEMG-ACC sensor fusion-proQuest. Canada: The University of Western Ontario, 2020.
[28] FANG Y F, LU H Q, LIU H. Multi-modality deep forest for hand motion recognition *via* fusing sEMG and acceleration signals. International Journal of Machine Learning and Cybernetics, 2023, 14(4): 1119-1131.
[29] SIMÃO M, MENDES N, GIBARU O, et al. A review on electromyography decoding and pattern recognition for human-machine interaction. IEEE Access, 2019, 7: 39564-39582.
[30] CLANCY E A, MORIN E L, HAJIAN G, et al. Tutorial. Surface electromyogram (sEMG) amplitude estimation: Best practices. Journal of Electromyography and Kinesiology, 2023, 72: 102807.
[31] BAN C Q, LIN M X, CHEN L, et al. Research on information acquisition and preprocessing of array force sensor//2018 15th International Conference on Ubiquitous Robots, June 26-30, 2018, Honolulu, HI, USA. New York: IEEE, 2018: 83-87.
[32] CHEN Z W, TAN J X, LIU M H. Using EEG to decode upper limb movement: elbow flexion or extension//2023 2nd International Conference on Data Analytics, Computing and Artificial Intelligence, October 17-19, 2023, Zakopane, Poland. New York: IEEE, 2023: 795-800.
[33] LESERRI D, GRIMMELSMANN N, MECHTENBERG M, et al. Evaluation of sEMG signal features and segmentation parameters for limb movement prediction using a feedforward neural network. Mathematics, 2022, 10(6): 932.
[34] YADAV S, KUMAR SAHA S, KAR R. Design of robust adaptive Volterra noise mitigation architecture for sEMG signals using metaheuristic approach. Expert Systems with Applications, 2023, 221: 119732.
[35] COSTA-GARCÍA Á, ITKONEN M, YAMASAKI H, et al. A novel approach to the segmentation of sEMG data based on the activation and deactivation of muscle synergies during movement. IEEE Robotics and Automation Letters, 2018, 3(3): 1972-1977.
[36] SHI X, QIN P J, ZHU J Q, et al. Feature extraction and classification of lower limb motion based on sEMG signals. IEEE Access, 2020, 8: 132882-132892.

利用表面肌电和阵列柔性薄膜压力传感器进行运动意图识别

卜令宇[1], 尹相国[1,2], 林明星[1*], 刘佳和[3]

1. 山东大学 机械工程学院 机械工程国家级实验教学示范中心 高效洁净机械制造教育部重点实验室, 山东 济南 250061;
2. 康复大学 康复科学与工程学院, 山东 青岛 266071;
3. 山东第二医科大学 康复医学院, 山东 潍坊 261053

摘　要： 运动意图识别被视为提升脑卒中患者上肢康复机器人训练效果的关键技术，但传统识别系统难以同时兼顾实时性与可靠性。为实现上肢运动意图的实时精准识别，本文提出一种基于表面肌电信号（sEMG）与阵列式柔性薄膜压力（AFTFP）传感器的多模态融合方法。通过对10名健康受试者（5男/5女，年龄23±2岁）进行肘关节屈伸、肩关节内外旋动作的测试实验，同步采集sEMG信号与人机交互力（HMIF）信号。将基于动态校准补偿的AFTFP信号与sEMG信号进行特征提取与融合处理，并采用支持向量机（SVM）对比单信号与融合信号的识别性能。实验结果表明：sEMG信号始终比HMIF信号提前175±25 ms出现（$p<0.01$，配对t检验）；离线条件下融合信号在不同时间窗下的识别准确率均超过99.77%；在0.1 s时间窗下，融合信号的实时识别准确率较单一sEMG信号提升14.1%，系统端到端延迟降至100 ms以内。AFTFP传感器首次被应用于运动意图识别，其低成本、高密度阵列设计为康复机器人提供了创新解决方案。研究结果证明，sEMG信号与HMIF信号的融合兼具两者优势，能实现实时精准的运动意图识别，为脑卒中康复等场景的人机交互提供高效指令输出。

关键词： 上肢康复机器人；运动意图识别；表面肌电信号；阵列柔性薄膜压力传感器；人机交互力

引用格式： BU Lingyu, YIN Xiangguo, LIN Mingxing, et al. Motion intention recognition using surface electromyography and arrayed flexible thin-film pressure sensors. Journal of Measurement Science and Instrumentation, 2025, 16(4): 486-497. DOI: 10.62756/jmsi.1674-8042.2025047